Functional Monochalcogenides: Raman Evidence Linking Properties, Structure, and Metavalent Bonding

Christophe Bellin,[1,*] Amit Pawbake,[1,2,*] Lorenzo Paulatto,[1] Keevin Béneut,[1] Johan Biscaras,[1] Chandrabhas Narayana,[3] Alain Polian,[1] Dattatray J. Late,[4] and Abhay Shukla[1,†]

[1]*Institut de Minéralogie, de Physique des Matériaux et de Cosmochimie, Sorbonne Université, UMR CNRS 7590, MNHN, 4 Place Jussieu, F-75005 Paris, France*

[2]*Institut Neel CNRS/UGA UPR2940, MCBT, 25 rue des Martyrs BP 166, 38042 Grenoble cedex 9, France*

[3]*Chemistry and Physics of Materials Unit, School of Advanced Materials, Jawaharlal Nehru Centre for Advanced Scientific Research, Jakkur, Bangalore 560 064, India*

[4]*Centre for Nanoscience and Nanotechnology Amity University Maharashtra, Mumbai- Pune Expressway, Bhatan, Post Somatne, Panvel, Mumbai, Maharashtra 410206, India*

(Received 25 March 2020; revised 17 August 2020; accepted 9 September 2020; published 28 September 2020)

Pressure- and temperature-dependent Raman scattering in GeSe, SnSe, and GeTe for pressures beyond 50 GPa and for temperatures ranging from 78 to 800 K allow us to identify structural and electronic phase transitions, similarities between GeSe and SnSe, and differences with GeTe. Calculations help to deduce the propensity of GeTe for defect formation and the doping that results from it, which gives rise to strong Raman damping beyond anomalous anharmonicity. These properties are related to the underlying chemical bonding and consistent with a recent classification of bonding in several chalcogenide materials that puts GeTe in a separate class of "incipient" metals.

DOI: 10.1103/PhysRevLett.125.145301

Recent work aiming to classify chalcogenides on the basis of several calculated or measured properties has led to the conclusion that anomalous behavior in potential materials for thermoelectric or phase change applications can be largely ascribed to a specific type of chemical bonding.

The link to a specific "resonant" bonding mechanism was first suggested by Lucovsky and White for GeTe [1], generalized and refined in subsequent works with respect to dielectric properties [2], bonding [3], and thermal properties [4]. Using coordination number, anharmonicity, bond polarizability, and conductivity to classify materials, this "metavalent" bonding [5,6] was identified as different from the classical resonant bonding and is now thought to be emblematic for certain properties like transport or optical contrast in these materials [7,8], defined by the competition between electronic localization in insulating ionic or covalent solids and delocalization in conducting metals. Phenomena like anharmonicity, on the other hand [5], are exacerbated and should show up in pressure and temperature dependence of phonon modes.

Here we provide spectroscopic evidence in the form of pressure- and temperature-dependent Raman measurements in GeSe, SnSe, and GeTe. In these IV–VI materials, the column IV and column VI elements are neighbors and the resulting binary compounds form a good basis for comparison of properties. The prototype phase change material GeTe is rhombohedral in ambient conditions and transits to a cubic NaCl structure and then to an orthorhombic structure as pressure increases [9]. A metastable cubic NaCl phase is also found in ambient conditions. GeSe and SnSe are known to undergo orthorhombic to orthorhombic transitions at low pressure as well as semiconductor to metal transitions. SnSe, meanwhile, is claimed to be a promising thermoelectric material at high temperature [10]. We compare pressure-dependent Raman spectra in SnSe and GeSe and find them to be remarkably similar. Their behavior is markedly different from our earlier findings in GeTe [9]. We also compare temperature-dependent Raman spectra between GeSe and GeTe and find a strong contrast. GeSe shows standard temperature-dependent softening and broadening and no phase change. GeTe shows anomalous softening and broadening and a high temperature phase change, all of which can be linked to the formation of Ge vacancies and ultimately to the unique bonding mechanism in this material.

Much of past work in these materials has been accomplished using x-ray and neutron diffraction. Raman spectroscopy is complementary to structural studies and sensitive to aspects like anharmonicity, electron phonon coupling, and isostructural or subtle phase changes, as our recent study on the pressure phase diagram of GeTe has shown [9]. A study of the ambient pressure phases of GeSe found an orthorhombic to cubic phase transition at 651 °C, just below the melting temperature of 670 °C [11]. Pressure studies confirm the persistence of the orthorhombic phase [12] or find a continuous *Pmcn* to *Ccmm* transition [13], notably accompanied by a sharp drop in resistance between 20 and 25 GPa.

SnSe at ambient pressure undergoes a transition within the orthorhombic structure from *Pnma* to *Cmcm* complete at about 800 K [14–16]. Most high pressure studies indicate similar subtle transitions. Indeed, the same transition is found at about 10 GPa by high pressure x-ray diffraction and Raman studies [16,17]. Another study [18] finds this transition at around 15 GPa with the appearance of a cubic phase at 27 GPa in a gradual evolution, which is complete only beyond 45 GPa. Calculations [19,20] find the *Pnma* to *Cmcm* transition at low pressure (2.5–6 GPa) and a transition to the cubic phase at high pressures nearing 40 GPa, while a lone study reported a transition to an unusual $P21/c$ structure at 12.6 GPa [21].

All monochalcogenide single crystals were purchased from 2D Semiconductors (USA). For high pressure measurements, a freshly cleaved flake was loaded in a membrane diamond anvil cell (DAC) [22] using a Rhenium gasket with a 250 μm diamond culet and neon as the pressure transmitting medium [23]. Neon ensures quasihydrostatic conditions, has no Raman activity, and is chemically inert, avoiding surface contamination in the pressure cell. The $R1$-line emission of a ruby [24] was used for pressure calibration [25]. A Jobin-Yvon HR-460 spectrometer (1500 grooves/mm monochromator and Andor CCD camera, spectrometer resolution being 1.5 cm^{-1}) in backscattering geometry was used for the Raman scattering experiments.

The primary beam was from a 514.5 nm Ar laser focused into a 2 μm spot. Incident power on the DAC was limited below 40 mW (and 120 mW for high pressure phases). The 12 cm^{-1} low frequency cutoff, crucial for many low frequency peaks, was achieved with Rayleigh rejection using three volume Bragg filters. A remnant low energy tail was subtracted using a polynomial background. For temperature-dependent Raman spectra, the sample was placed in a water-cooled Linkam TS1500 stage in a flow of pure argon. The ambient and high pressure data were recorded in the range of 12–1200 cm^{-1} and acquired for 120–900 s per pressure point depending on count rate.

All calculations were performed using the QUANTUM ESPRESSO suite of codes [26,27], including phonons and Raman cross sections from perturbation theory [28,29] and anharmonic properties using D3Q codes [30]. For all the simulations we used norm-conserving pseudopotentials from the SG15-Optimized Norm-Conserving Vanderbilt library library [31,32] and the Perdew-Burke-Ernzerhof gradient-corrected local functional with van der Waals Grimme-D2 correction [33,34]. The Fourier transform grid was kept constant at different pressures to ensure consistency. In the worst case (larger cell), it corresponds to a kinetic energy cutoff of at least 60 Ry. For sampling the electronic reciprocal space, we used a $4 \times 4 \times 4$ grid for the *Cmcm* structure and four points along the short cell directions and two points along the long ones for the *Pcmn* and *Pnma* structures. For the phonon-phonon interaction calculation in GeTe, we computed the second and third dynamical matrices over $8 \times 8 \times 8$ and $4 \times 4 \times 4$ grid points, respectively. In order to integrate the spectral weight equation [35,36], the matrices were then converted to two- and three-body force constants and Fourier interpolated over a grid of $70 \times 70 \times 70$ points.

Ambient pressure and temperature phases of bulk GeSe and SnSe are orthorhombic with 8 atoms per unit cell [37] and 12 Raman active modes ($4A_g + 2B_{1g} + 4B_{2g} + 2B_{3g}$). The $4B_{2g}$ modes are difficult to detect due to a weak Raman tensor, but the B_{1g} modes (GeSe) and the B_{3g} modes (SnSe) can be observed for unpolarized Raman backscattering spectra along the c axis, as seen in the lowest pressure spectra of Figs. 1(a) and 1(c), which are in good agreement with previous reports at ambient conditions [38–40]. The modes are symmetry indexed in Figs. 1(b) and 1(d). In many previous reports, low energy phonons remained undetected, often due to instrumental reasons [39–41].

As can be seen in Fig. 1, the pressure variation is remarkably similar in GeSe and SnSe. It is, however, markedly different for GeTe, as reported in our recent work [9]. The Raman signal vanishes with pressure in both GeSe and SnSe, beyond approximately 35 GPa in GeSe and beyond 10 GPa in SnSe, though a couple of modes survive to about 50 GPa. $A_g{}^1$, $A_g{}^3$, B_{1g}, and B_{3g} modes in both materials behave anomalously, with little dispersion, first

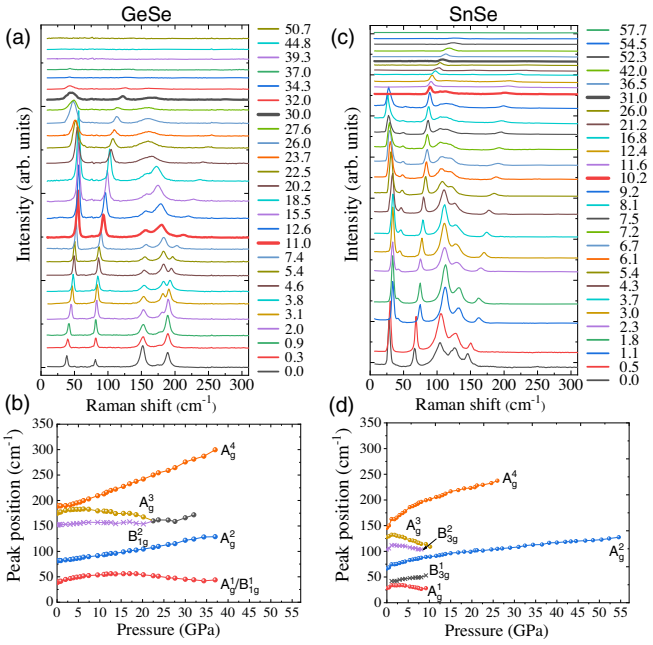

FIG. 1. Pressure-dependent Raman spectra of (a) GeSe and (b) SnSe, showing the pressure dependence of A_g modes (dots) and B_{1g} and B_{3g} modes (crosses). Pressure increases from bottom to top and values are in GPa. The Raman spectra around 10 and 30 GPa are shown with a thick line to enable easy comparison between the two materials. Extracted Raman shifts and their pressure variation for (c) GeSe and (d) SnSe show the overall similarity of the two materials.

hardening and then softening as pressure increases. A_g^2, A_g^4 modes show a monotonous hardening. The vanishing Raman signal is probably due to strong damping from increasing carrier concentration and electronic transition to a small gap semiconductor or a semimetal. The ambient condition band gap is 2.29 eV in GeSe and 1.79 eV in SnSe. The Raman signal could also disappear due to a phase transition to a cubic phase, though this seems to be excluded from earlier diffraction work for GeSe [12,13]. As detailed above, in GeSe some diffraction studies do evoke a structural transition from the *Pmcn* to the *Cmcm* space group [13], while others [12] do not. From our Raman data, we cannot detect any such structural change. *Ab initio* calculations indicate that the *Pnma* and the higher symmetry *Cmcm* structures are very similar, but do rule out the possibility of the trigonal structure, which only has two active modes (see Supplemental Material [42]). Similarly, in SnSe, an experimental x-ray diffraction study finds a gradual transition from ambient pressure *Pnma* to *Cmcm*, complete at 10.5 GPa [17].

Since only two weak Raman lines persist above this pressure in our data, and *Cmcm* is a structure with higher symmetry, our data are compatible with this scenario. A cubic CsCl phase has been reported in SnSe at a pressure of 27 GPa [18] with the transition completed at 45 GPa, consistent with some simulations [19,20] and with the disappearing Raman signal at these high pressures in our work. From *ab initio* simulation, the *Cmcm* phase becomes increasingly symmetric with pressure. However, calculated Raman cross sections can vary enormously, as mentioned earlier, and a further complication arises because the system is metallic above 10 GPa at the Density Functional Theory, local-density approximation level.

Beyond these similarities, some differences exist. In GeSe, though the Raman signal completely disappears only beyond 35 GPa, there is an abrupt drop in the intensity of the Raman lines and a corresponding broadening at a pressure of 20 GPa, signifying increased damping (see Supplemental Material [42]). Interestingly, transport measurements as a function of pressure in GeSe show that, though the resistance drops continuously with pressure over several orders of magnitude, there is an abrupt drop between 20 and 25 GPa [12,13], signifying a change in electronic structure. The increased damping of the Raman lines could be due to an increase in charge carriers, as seen in several experimental and theoretical studies of doping in semiconductors [43–46].

In SnSe we detect a discontinuous change in Raman frequencies of all modes with a jump of 12% at 1.1 GPa. Though theoretical studies evoke a low pressure structural change (*Pnma* to *Cmcm* [19,20]), the Raman spectrum remains identical, indicating an isostructural transition at this low pressure. In summary, in GeSe, the structure remains orthorhombic *Pnma*, but pressure induces metallicity and an abrupt damping of Raman peaks is observed at 20 GPa, with complete disappearance of the Raman signal between 35 and 40 GPa. In SnSe, an isostructural transition within the *Pnma* structure is seen at 1.1 GPa. At 10 GPa, a transition to the *Cmcm* structure is probable. Between 27 and 55 GPa, the single remnant Raman peak disappears, which is interpreted as a transition to a cubic structure with accompanying metallicity [18].

Finally, we come back to the observation (Fig. 1) that A_g^1, A_g^3, B_{1g}, and B_{3g} modes in both GeSe and SnSe disperse little, with visible softening for some modes as pressure increases. Softening is accompanied by line broadening and damping (see Supplemental Material [42]) and, as we have pointed out above, these can be explained by an increasing metallic nature of the materials. These observations are compatible with a change in the prevalently covalent bonding of these materials toward metavalent bonding. In effect, both materials should increasingly move toward an incipient metallic state with increasing pressure because pressure induced electron delocalization reduces both electron transfer (ionicity) and sharing (covalency). Furthermore, as observed experimentally, this should happen at lower pressures for SnSe than for GeSe, which is more covalent and has a lower conductivity in ambient conditions [5,6].

The dependence on temperature for SnSe can be consulted in several recent studies (for example, [40]). Clearly, all modes in SnSe broaden with temperature, testifying to strong anharmonicity. In SnSe, an orthorhombic *Pnma* to *Cmcm* transition takes place around 800 K with the disappearance of some modes in the more symmetric *Cmcm* structure, which is, however, not Raman silent because the A_g^2 mode persists. In Fig. 2, we show the temperature variation of the Raman signal for GeTe [Fig. 2(a)] and GeSe [Fig. 2(b)]. GeSe shows standard behavior as Raman modes soften marginally and broaden with temperature, in keeping with lattice expansion and increasing anharmonicity. No change in crystal structure can be seen and none is expected since the transition to the cubic phase occurs at higher temperature. GeTe, on the other hand, shows anomalous broadening of its two modes, even at low temperature. The broadening increases considerably beyond 300 K, and beyond 550 K the two distinct maxima are lost in a broad and very low intensity background, which shifts to higher energy between 600 and 800 K.

It must be remembered that beyond 700 K a transition to the Raman silent cubic structure takes place. The 300 K measurement before heating (black line) and after cooling down (green line) are quite similar, showing that the high temperature phase transition is reversible. However, small differences can be distinguished between the two spectra in the region between 100 and 250 cm^{-1}. The significance of this small difference will be discussed below, where we show that the temperature broadening and evolution of the Raman signal for GeTe is anomalous.

In Fig. 3(a), the ambient pressure Raman spectra of the three materials at 300 K are shown. GeSe and SnSe spectra

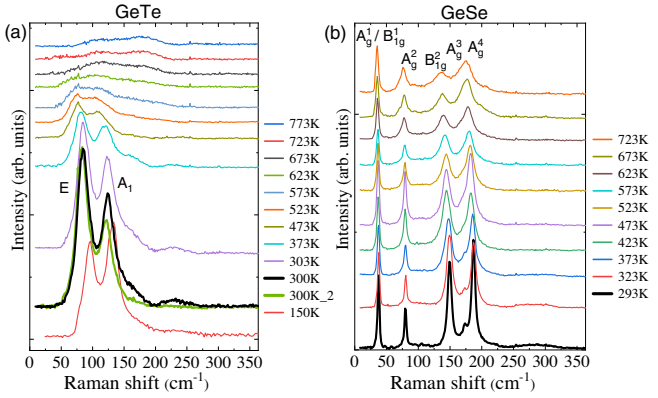

FIG. 2. Temperature-dependent Raman spectra of (a) GeTe and (b) GeSe. The room temperature spectra are different because of the different crystal structure (rhombohedral for GeTe and orthorhombic for GeSe). The variation with temperature is also very different, with the anomalously broad peaks getting broader in GeTe and eventually disappearing in the high temperature Raman silent cubic phase. The 300 K spectra for GeTe correspond to the measurement before heating (black line) and after cooling down to room temperature (green line). In GeSe, the structure remains unchanged to the highest measured temperature, and peaks expectedly soften and broaden with temperature.

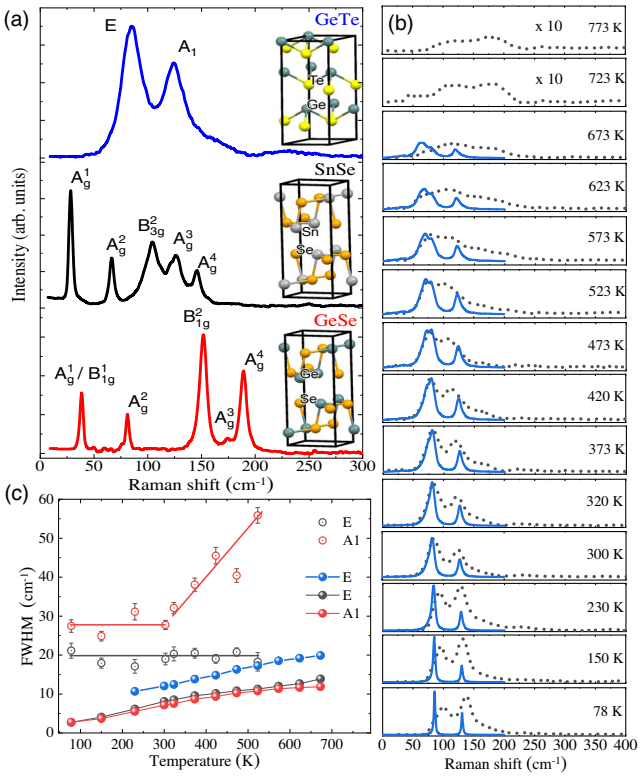

FIG. 3. (a) Ambient pressure, room temperature Raman spectra for GeSe, SnSe, and GeTe, with the ambient condition rhombohedric $R3m$ unit cell shown for GeTe and the orthorhombic $Pnma$ unit cell shown for GeSe and SnSe. (b) Temperature dependence of experimental GeTe Raman spectra (dotted line, measured count rate) and a comparison with calculation including anharmonicity (solid line, normalized to experimental count rate). (c) Extracted variation (full width at half maximum) with temperature of experimental (empty circles) and simulated (full circles) linewidths in (b). The doubly degenerate E mode splits with temperature in simulation.

are similar, while GeTe is different, because of a different crystalline structure, but, more importantly, because phonon linewidth is much bigger. In Fig. 3(b), the temperature variation of the GeTe Raman spectrum is compared to calculation. The simulation includes the frequency-dependent two-phonon processes allowed by anharmonic phonon-phonon interaction [35], which is important in these materials, as well as thermal expansion. Other contributions to linewidth broadening, not included in the simulation, are electron-phonon scattering and scattering by lattice defects. In Fig. 3(c), the variation of the experimental and simulated linewidths is shown. The simulation reveals that at low temperature the anharmonic contribution is small, as expected. The measured linewidths are significantly broader than the simulated ones and independent of temperature below 300 K, indicating that the other contributions to linewidth are important. Above 600 K, the experiment corresponds to a low intensity background. Above 700 K, where a transition to the Raman silent cubic phase takes place, the background shifts to higher energy. Even at the lowest temperatures, a high energy shoulder exists between 150 and 200 cm^{-1}, which is not accounted for in the calculations. This shoulder transforms to a major part of the background at high temperature and in the cubic phase.

A part of the broadening over the whole temperature range, and the low intensity, high energy background in the Raman silent cubic phase can be both traced to the high propensity of GeTe to form Ge vacancies, particularly in the cubic structure [47].

Metavalent bonding is characterized by a relative ease in bond breaking, which facilitates vacancy formation [48]. Indeed, calculations [49,50] and experiments [15,40] indicate that large scale Ge vacancies are very easily formed in GeTe and should contribute to phonon linewidth through scattering [46]. Edwards *et al.* [50] show that Ge vacancies have a formation energy that is a third of Te vacancies, and they do not induce localized gap states but delocalized states at the top of the valence band, giving rise to p-type metallic conductivity. Screening from this charge softens phonons [45] and will also contribute to Raman linewidth broadening. Finally, Park *et al.* [51] have shown that local Te rich phases can exhibit a variety of modes with energies ranging between 120 and 170 cm^{-1}, the range of the background signal in our high temperature Raman spectra. These modes originate in Te—Te bonds (induced by Ge vacancies) and $GeTe_4$ edge sharing octahedra. A further point to be noted is that, though we recover the Raman signal at 300 K after having cooled the sample down [Fig. 2(a)], ensuring that the measured high temperature changes are not due to extrinsic effects, differences appear in the high energy region

between 100 and 200 cm^{-1}, which corresponds to the signal from defects. Ge vacancies and the accompanying doping can thus explain the temperature dependence and the anomalous broadening of the Raman spectra in GeTe, for which anharmonic effects alone cannot account.

The peculiar properties of GeTe and other tellurides like SnTe or PbTe have been highlighted by a recent classification of their chemical bonding, which sets them apart from GeSe or SnSe [5,6] as incipient metals with a metavalent bonding mechanism different from that of ionic or covalent solids or of conventional metals. This classification can be important for material design and understanding if it can be validated by experiment. Our pressure- and temperature-dependent, high resolution, low frequency Raman scattering results are consistent with this classification because they confirm the similarity of GeSe and SnSe and the singularity of GeTe. Temperature-dependent Raman scattering experiments and simulations show that the anomalous broadening of the Raman lines observed in GeTe cannot be explained by anharmonicity alone. It is a sign of the peculiar chemical bonding in this material and a defect prone structure, known to result in strong doping and resultant phonon damping. On the other hand, pressure-dependent Raman spectra show the close similarity between the covalently bonded solids SnSe and GeSe. They also reveal the intriguing possibility that, at higher pressure, SnSe and GeSe evolve in the direction of incipient metals, with anharmonic phonons, higher conductivity, and metavalent bonding. This Letter also helps establish the relevant phase diagrams of all these materials, many aspects of which needed clarification.

This work was granted HPC resources of IDRIS under GENCI Project No. 7320. A. P. acknowledges the Indo-French Centre for the Promotion of Advanced Research (CEFIPRA, Grant No. 5608-2) for Raman-Charpak and postdoctoral fellowship.

*These authors contributed equally to this work.
†abhay.shukla@sorbonne-universite.fr

[1] G. Lucovsky and R. M. White, Phys. Rev. B **8**, 660 (1973).
[2] K. Shportko, S. Kremers, M. Woda, D. Lencer, J. Robertson, and M. Wuttig, Nat. Mater. **7**, 653 (2008).
[3] D. Lencer, M. Salinga, B. Grabowski, T. Hickel, J. Neugebauer, and M. Wuttig, Nat. Mater. **7**, 972 (2008).
[4] S. Lee, K. Esfarjani, T. Luo, J. Zhou, Z. Tian, and G. Chen, Nat. Commun. **5**, 3525 (2014).
[5] M. Wuttig, V. Deringer, X. Gonze, C. Bichara, and J. Raty, Adv. Mater. **30**, 1803777 (2018).
[6] J. Raty, M. Schumacher, P. Golub, V. Deringer, C. Gatti, and M. Wuttig, Adv. Mater. **31**, 1806280 (2019).
[7] B. Huang and J. Robertson, Phys. Rev. B **81**, 081204(R) (2010).
[8] B. J. Kooi and M. Wuttig, Adv. Mater. **32**, 1908302 (2020).
[9] A. Pawbake, C. Bellin, L. Paulatto, K. Béneut, J. Biscaras, C. Narayana, D. J. Late, and A. Shukla, Phys. Rev. Lett. **122**, 145701 (2019).
[10] C. W. Li, J. Hong, A. F. May, D. Bansal, S. Chi, T. Hong, G. Ehlers, and O. Delaire, Nat. Phys. **11**, 1063 (2015).
[11] H. Wiedemeier and P. A. Siemers, Z. Anorg. Allg. Chem. **411**, 90 (1975).
[12] A. Onodera, I. Sakamoto, Y. Fujii, N. Móri, and S. Sugai, Phys. Rev. B **56**, 7935 (1997).
[13] M. Xu, S. Jakobs, R. Mazzarello, J. Cho, Z. Yang, H. Hollermann, D. Shang, X. Miao, Z. Yu, L. Wang, and M. Wuttig, J. Phys. Chem. C **121**, 25447 (2017).
[14] L. Zhao, S. Lo, Y. Zhang, H. Sun, G. Tan, C. Uher, C. Wolverton, V. Dravid, and G. Kanatzidis, Nature (London) **508**, 373 (2014).
[15] T. Chattopadhyay, J. Pannetier, and H. G. Von Schnering, J. Phys. Chem. Solids **47**, 879 (1986).
[16] I. Efthimiopoulos, M. Berg, A. Bande, L. Puskar, E. Ritter, W. Xu, A. Marcelli, M. Ortolani, M. Harms, and J. Müller, Phys. Chem. Chem. Phys. **21**, 8663 (2019).
[17] I. Loa, R. J. Husband, R. A. Downie, S. R. Popuri, and J. W. Bos, J. Phys. Condens. Matter **27**, 072202 (2015).
[18] X. Chen, P. Lu, X. Wang, Y. Zhou, C. An, Y. Zhou, C. Xian, H. Gao, Z. Guo, C. Park, B. Hou, K. Peng, X. Zhou, J. Sun, Y. Xiong, Z. Yang, D. Xing, and Y. Zhang, Phys. Rev. B **96**, 165123 (2017).
[19] K. Nguyen-Cong, J. Gonzalez, B. Steele, and I. Oleynik, J. Phys. Chem. C **122**, 18274 (2018).
[20] H. Yu, W. Lao, L. Wang, K. Li, and Y. Chen, Phys. Rev. Lett. **118**, 137002 (2017).
[21] J. Yan, F. Ke, C. Liu, L. Wang, Q. Wang, J. Zhang, G. Li, Y. Han, Y. Ma, and C. Gao, Phys. Chem. Chem. Phys. **18**, 5012 (2016).
[22] J. C. Chervin, B. Canny, J. M. Besson, and P. Pruzan, Rev. Sci. Instrum. **66**, 2595 (1995).
[23] B. Couzinet, N. Dahan, G. Hamel, and J. Chervin, High Press. Res. **23**, 409 (2003).
[24] J. C. Chervin, B. Canny, and M. Mancinelli, Int. J. High Pressure Res. **21**, 305 (2001).
[25] J. D. Barnett, S. Block, and G. J. Piermarini, Rev. Sci. Instrum. **44**, 1 (1973).
[26] P. Giannozzi *et al.*, J. Phys. Condens. Matter **29**, 465901 (2017).
[27] P. Giannozzi *et al.*, J. Phys. Condens. Matter **21**, 395502 (2009).
[28] S. Baroni, S. De Gironcoli, A. Dal Corso, and P. Giannozzi, Rev. Mod. Phys. **73**, 515 (2001).
[29] M. Lazzeri and F. Mauri, Phys. Rev. Lett. **90**, 036401 (2003).
[30] L. Paulatto, F. Mauri, and M. Lazzeri, Phys. Rev. B **87**, 214303 (2013).
[31] D. R. Hamann, Phys. Rev. B **88**, 085117 (2013).
[32] M. Schlipf and F. Gygi, Comput. Phys. Commun. **196**, 36 (2015).
[33] J. P. Perdew, K. Burke, and M. Ernzerhof, Phys. Rev. Lett. **77**, 3865 (1996).
[34] S. Grimme, J. Comput. Chem. **27**, 1787 (2006).
[35] L. Paulatto, I. Errea, M. Calandra, and F. Mauri, Phys. Rev. B **91**, 054304 (2015).
[36] R. A. Cowley, Rep. Prog. Phys. **31**, 123 (1968).

[37] A. Okazaki, J. Phys. Soc. Jpn. **13**, 1151 (1958).
[38] H. R. Chandrasekhar, R. G. Humphreys, U. Zwick, and M. Cardona, Phys. Rev. B **15**, 2177 (1977).
[39] H. B. Ribeiro, S. L. L. M. Ramos, L. Seixas, C. J. S. de Matos, and M. A. Pimenta, Phys. Rev. B **100**, 094301 (2019).
[40] F. Liu, P. Parajuli, R. Rao, P. C. Wei, A. Karunarathne, S. Bhattacharya, R. Podila, J. He, B. Maruyama, G. Priyadarshan, J. R. Gladden, Y. Y. Chen, and A. M. Rao, Phys. Rev. B **98**, 224309 (2018).
[41] Y. Kim and I. Choi, J. Korean Phys. Soc. **72**, 238 (2018).
[42] See Supplemental Material at http://link.aps.org/supplemental/10.1103/PhysRevLett.125.145301 for simulations of pressure variation of Raman spectra in GeSe and SnSe and for evidence of damping of Raman modes with pressure.
[43] F. Cerdeira, T. A. Fjeldly, and M. Cardona, Phys. Rev. B **8**, 4734 (1973).
[44] D. Kumar, M. Chandrana, and M. S. Ramachandra Rao, Appl. Phys. Lett. **110**, 191602 (2017).
[45] R. Shaltaf, X. Gonze, M. Cardona, R. K. Kremer, and G. Siegle, Phys. Rev. B **79**, 075204 (2009).
[46] D. Campi, L. Paulatto, G. Fugallo, F. Mauri, and M. Bernasconi, Phys. Rev. B **95**, 024311 (2017).
[47] M. Sist, H. Kasai, E. M. J. Hedegaard, and B. B. Iversen, Phys. Rev. B **97**, 094116 (2018).
[48] M. Zhu, O. Cojocaru-Mirédin, A. Mio, J. Keutgen, M. Küpers, Y. Yu, J. Cho, R. Dronskowski, and M. Wuttig, Adv. Mater. **30**, 1706735 (2018).
[49] W. Wełnic, A. Pamungkas, R. Detemple, C. Steimer, S. Blügel, and M. Wuttig, Nat. Mater. **5**, 56 (2006).
[50] A. H. Edwards, A. C. Pineda, P. A. Schultz, M. G. Martin, A. P. Thompson, H. P. Hjalmarson, and C. J. Umrigar, Phys. Rev. B **73**, 045210 (2006).
[51] J. Park, M. Song, S. Yoon, H. Lim, D. Jeong, C. Cheong, and H. Lee, Phys. Status Solidi A **210**, 267 (2013).